

Stabilized double-electron capture in Kr^{q+} ($q = 17, 18$)–Kr collisions

S. Martin, A. Denis, A. Delon, and J. Désesquelles

*Laboratoire de Spectrometrie Ionique et Moleculaire, Université Claude Bernard Lyon 1,
Campus de la Doua, F-69622 Villeurbanne CEDEX, France*

Y. Ouerdane

*Laboratoire de Traitement du Signal et Instrumentation, Université de Saint-Etienne,
23 rue du Dr. Paul Michelon, F-42023 Saint-Etienne, France*

(Received 3 February 1993)

We have determined the distribution of n states initially populated in a double- or multielectron-capture collision of Kr^{q+} ($q = 17, 18$) with Kr at low energy (≈ 5 keV/u). Radiative decay curves of Rydberg transitions of the projectile ions were obtained by translating the target gas jet along the projectile beam. As a result for Kr^{18+} projectiles, we found that an initial population of Kr^{16+} equally distributed from $n = 14$ to 19 allows the observed Kr XVII 13-14 radiative decay curve to be reproduced relatively well. Furthermore, coincidence time-of-flight spectroscopy of photons emitted by recoil ions of given charge states was used to measure the radiative decay of recoil-ion transitions. From the Kr VII $7i-8k$ decay curve we deduced an initial population distribution of the Kr^{6+} recoil ion centered around $n = 20$. These results lead to a better understanding of the mechanisms of double-electron capture responsible for populating Rydberg states, especially those in asymmetric configurations.

PACS number(s): 34.70.+e, 34.50.Fa

I. INTRODUCTION

States selectively populated through single-electron capture by highly charged ions from a rare-gas target are well reproduced by *ab initio* calculations [1]. Multielectron-capture processes assume at least two active electrons and calculations are obviously more complex. For multielectron targets *ab initio* calculations are rather successful in predicting double-capture cross sections and final doubly excited-state (n, n') populations [2]. However, true double capture (TDC) (i.e., two electrons are captured and stabilized on the projectile) cannot be predicted for a high charge state of the projectile [3]. For more than two active electrons, independent-particle models have been developed such as the extended classical barrier model (ECBM) [4]. The ECBM predicts the principal quantum numbers n of the captured electrons and the total cross sections [5].

In recent papers [6,7] we reported an analysis of visible photons emitted after double and multicapture processes. If double-capture processes are selected by coincidence between photons and recoil ions, the transitions corresponding to two stabilized electrons are interpreted as Rydberg transitions issued from asymmetrical configurations ($n \ll n'$) [8]. This finding establishes that double-capture processes can populate both symmetrical ($n \approx n'$) and asymmetrical ($n \ll n'$) configurations. For high-lying states, symmetrical configurations are generally autoionizing, while asymmetrical configurations can stabilize radiatively through Rydberg transitions. Recently, energy gain and angular spectroscopy by Roncin *et al.* [9] confirmed that a part of TDC is due to asymmetrical configuration populations in the case of $\text{O}^{8+} + \text{Ar}$ collisions. They also found that the angular diffusion

profiles are identical for autoionizing double capture and TDC processes, suggesting that both proceed through the same primary mechanism. As the projectile comes in, the (4,4) configuration is populated and then, as the projectile leaves, a second mechanism can feed the (3, n) configurations from the (4,4) configurations. More precisely, as the projectile leaves, the potential-energy curve of the (4,4) autoionizing state crosses the (3, n) potential-energy curves [10]. This mechanism populates the “top” of the asymmetrical configurations. These configurations are the (3,high n) configurations in $\text{O}^{8+} + \text{Ar}$ collisions. Moreover, this Rydberg electron can be recaptured by the target in a highly excited state. We demonstrated [6,7] the recapture of Rydberg electrons by the target atom by observing Rydberg transitions of high-charge-state recoil ions.

In this paper we present an analysis of the decay curves of Rydberg transitions issued from double-capture processes. Initial populations on the projectile or on the target are deduced from radiative decay curves using a cascade model.

II. EXPERIMENTAL SETUP

Kr^{17+} and Kr^{18+} ions were produced by an ECR source at energies of 340 and 360 keV, respectively. The experimental setup shown in Fig. 1 is the same as in [8] except for the gas target and the photon analysis. A narrow slit which is tunable from outside from 5 to 200 μm and a circular hole (200 μm diameter), located at about 10 and 3 cm, respectively, before the interaction region, considerably reduce the angular dispersion of the incoming beam. An X, Y, Z carriage allows the precise movement of a 1-mm-diameter needle. The gas pressure mea-

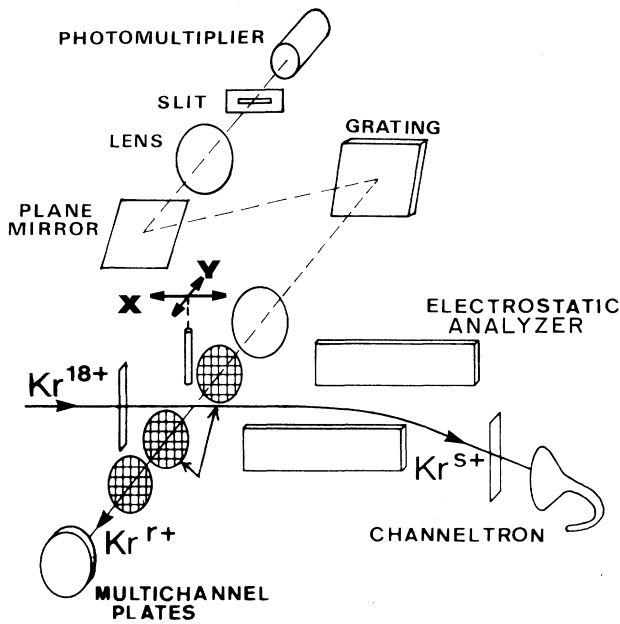


FIG. 1. Experimental setup Kr^{18+} incident ions, Kr^{r+} recoil ions, Kr^{s+} stabilized ions. X carriage allows one to move the gas target and to record the radiative decay of a selected Rydberg transition.

sured before the nozzle by a Baratron gauge was varied by up to 1 mbar. The residual pressure inside the chamber is lower than 2×10^{-7} mbar. The gas target profile is measured by moving the carriage perpendicularly to the ion beam and by recording the total light intensity. As a result the length of interaction between the gas jet and the projectile beam is found to be about 2 mm. Recoil ions are extracted from the interaction region by a transverse homogeneous electric field of 100 V/cm and are then accelerated by the multichannel plate (MCP) detector. The observation axis of the spectrometer is perpendicular to the gas jet and to the ion beam. Photons are collected on an aspherical lens ($f/d=0.7$) and sent on a largely opened, specially constructed homemade spectrometer equipped with a 1200-line/mm grating blazed at 500 nm. The exit slit is parallel to the beam axis. A cooled EMI6256S photomultiplier detects the selected photons.

Projectiles emerging from the interaction region are selected in charge by a low-resolution electrostatic analyzer and are detected by a channeltron. Charge states of recoil ions are analyzed by time-of-flight measurements allowing coincidence measurements between projectile and recoil ions and between photons and ions. In the latter case, the photomultiplier provides the start pulse to a time-to-amplitude converter stopped by a signal from the anode of the MCP.

Two different techniques are used to determine the time evolution of photon emission depending on the source of light. To record the time evolution of projectile excited states, the gas jet is precisely moved upstream of the ion beam, across and away from the observation window, as in the beam-foil technique. Recorded curves be-

gin by a growing intensity corresponding to an increase in collisions along the path of ions inside the gas jet, reaching a maximum, and then decreasing in intensity corresponding to the free radiative decay outside the target. To study the radiative decay of target Rydberg states, the gas jet is kept fixed in front of the observation region and we measure by coincidence how long the space of time is between the emission of a wavelength-selected photon and the detection of the emitting recoil ion. In a time-of-flight spectrum the coincidence number increases as time increases. The space of time is indeed longer for the numerous ions emitting photons just after being excited because these early photons deliver start pulses earlier, although the stop pulse is delivered by the recoil ion at a given time. To be correctly determined, radiative decays should be shorter than the time-of-flight of ions inside the extraction zone and the observation window of the spectrometer. Previous tests with N_2^+ recoil ions demonstrated that radiative decay measurements are not perturbed up to 100 ns corresponding to a path of about 2 mm.

III. RESULTS AND DISCUSSION

The visible spectrum emitted from 300 to 600 nm after the $\text{Kr}^{18+} + \text{Kr}$ collision is shown in Fig. 2. Table I gives the identification of Rydberg transitions emitted by the projectiles after electron capture (Kr^{16+} to Kr^{12+}) and by the recoil ions (Kr VI 7-8 and Kr VII 7-8). It should be noted that the observed Rydberg transitions are principally due to transitions between high angular momentum states [7]. Measured wavelengths are compared with hydrogenic values. The agreement is fairly good and shows that the screening by the internal electrons can be neglected for the Kr XVII transitions. Spectra emitted after the $\text{Kr}^{17+} + \text{Kr}$ collision are shown in Fig. 3. In Fig. 3(a) the observation axis crosses the gas jet axis, while in Fig. 3(b) the observation axis crosses the ion beam 6 mm after the gas jet axis. Table II gives identifications of the observed transitions and comparisons of measured wavelengths with hydrogenic values.

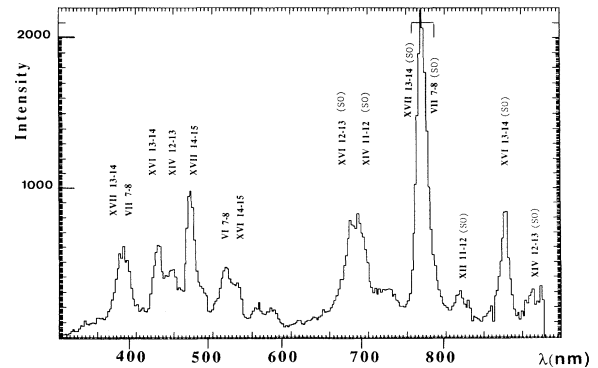


FIG. 2. Spectra of Rydberg transitions issued from multicapture processes by Kr^{18+} from Kr. The spectrometer observation axis is in the same plane as the gas jet axis. The acronym SO refers to lines measured in second order.

TABLE I. Identification of transitions measured in $\text{Kr}^{18+} + \text{Kr}$ collisions and comparison with predictions of hydrogenic calculations. Experimental error bar is about 2 nm. The acronym SO refers to lines measured in second order.

Transitions	Observed wavelength (nm)	Hydrogenic wavelength (nm)
XVII 13-14	387	386.8
VII 7-8		388.8
XVI 13-14	437	436.7
XIV 12-13	454	452.6
XVII 14-15	480	479.5
VI 7-8	525	529.2
XVI 14-15	542	541.3
XVI 12-13 (SO)	342 (SO)	346.5
XIV 11-12 (SO)	351 (SO)	352.2
XVII 13-14 (SO)	387 (SO)	386.8
VII 7-8 (SO)		388.8
XIII 11-12 (SO)	407 (SO)	408.5
XVI 13-14 (SO)	436 (SO)	436.7
XIV 12-13 (SO)	451 (SO)	452.6

TABLE II. Identification of transitions measured in $\text{Kr}^{17+} + \text{Kr}$ collisions and comparison with predictions of hydrogenic calculations. Experimental error bar is about 2 nm. The acronym SO refers to lines measured in second order.

Transitions	Observed wavelength (nm)	Hydrogenic wavelength (nm)
VII 708	387	388.8
XV 12-13		394.2
XVI 13-14	437	436.7
XIV 12-13	454	452.6
XV 13-14	496	496.8
VI 7-8	525	529.2
XVI 14-15	542	541.3
XIV 13-14	571	570.4
XVI 12-13 (SO)	342 (SO)	346.5
XIV 11-12 (SO)	351 (SO)	352.2
VII 7-8 (SO)	388 (SO)	388.8
XV 12-13 (SO)	395	394.2
XIII 11-12 (SO)	407 (SO)	408.5
XVI 13-14 (SO)	436 (SO)	436.7
XIV 12-13 (SO)	451 (SO)	452.6

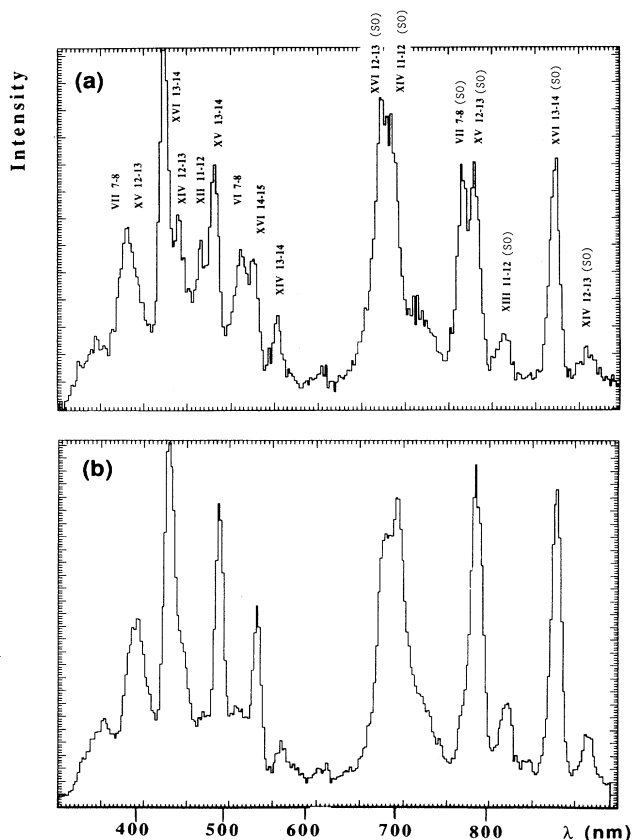


FIG. 3. Spectra of Rydberg transitions issued from multicapture processes by Kr^{17+} from Kr. The acronym SO refers to lines measured in second order. (a) The spectrometer observation axis is in the same plane as the jet axis. (b) The observation axis is fixed 6 mm behind the jet axis. Recoil-ion transitions disappear (Kr VI and Kr VII).

Of course, Kr VI 7-8 and Kr VII 7-8 transitions of recoil ions present in Fig. 3(a) disappear in Fig. 3(b). We observe weak variations in intensities of lines emitted by the projectile depending on the upper-level lifetime values, as observed in usual beam-foil spectroscopy for prompt and delayed spectra.

We measured and analyzed the decay curves of Kr XVII 14-15, Kr XVII 13-14, and Kr XVI 13-14 transitions in $\text{Kr}^{18+} + \text{Kr}$ collisions and Kr XVI 13-14, Kr XV 13-14 transitions in $\text{Kr}^{17+} + \text{Kr}$ collisions. We only present the decay curve of the Kr XVII 13-14 transition (Fig. 4). The Kr XVII 13-14 line is blended by the Kr VII 6-7 line from the target. However, the contribution of the target component is not so important since the intensity ratio was measured by analyzing the photon-recoil-ion coincidences [8] to be about 1:8. This weak component due to the Kr VII 6-7 transition was subtracted from the experimental decay curve. Results on high- n initial populations ($n \geq 14$) were deduced from the comparison of experimental and theoretical decays.

Theoretical decay curves were obtained by means of a n th-order Rydberg cascade model [11]. In this model, we used the hydrogenic transition probabilities, which are justified for high n and l quantum numbers, and we have only taken into account $\Delta l = -1$ radiative transitions ($n, l \rightarrow n-1, l-1$). Indeed, contributions due to the $\Delta l = 1$ transitions are in general very low and can be neglected here. In order to simulate the Kr XVII 13-14 decay, we calculated the contributions of all possible decay routes from $n=22$ to $n=14$ states (8th-order cascade). The most important contributions are the yrast cascades $(n, l = n-1 \rightarrow n-1, l = n-2 \rightarrow \dots \rightarrow 14, 13)$. We display in Fig. 5 theoretical radiative growing and decaying curves corresponding to primary population in single n levels ($n = 14, 16, 18, 19$), demonstrating how the cascading times induce delays in light emission and how

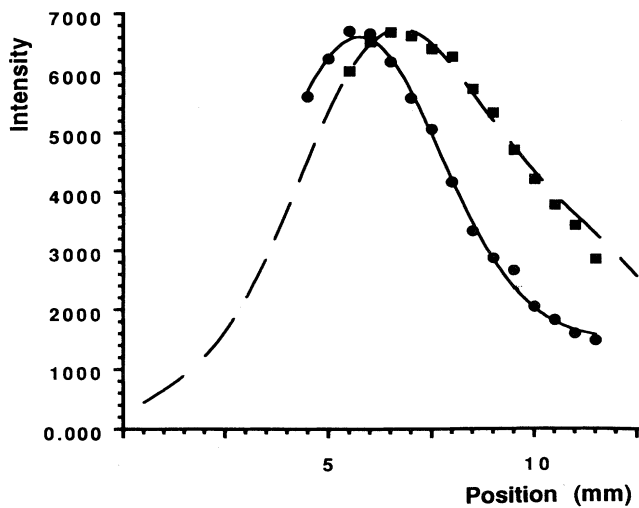


FIG. 4. Decay curve of the Kr XVII 13-14 transition. Shape (●) of the gas jet deduced from the intensity variation of the Kr VII 7-8 transition of the target. Observed (■) radiative decay of the Kr XVII 13-14 transition of the projectile. Simulated decay curve (—).

higher initial n levels induce slower decays. Several level population models have been taken into consideration: $(2l+1)n^{-3}$, l^2n^{-3} , n^{-2} . A preferential population of high angular momentum l of Rydberg states was demonstrated in the present ($v \approx 0.4$ a.u.) velocity regime [12]. The best agreement of the simulation with experimental intensity curves is obtained by assuming a constant population of $n = 14$ to 19 states and a $(2l+1)$ distribution for angular momentum l . Higher- n Rydberg cascades would give a contribution of the decay curve after about the 15-mm path (Fig. 5) and the corresponding population could not have been measured because the gas jet translation is restricted to 12 mm. This result shows that the n population in an asymmetrical double-electron capture spreads over numerous n values. For comparison, in the $\text{Kr}^{18+} + \text{Kr}$ case, ECBM indicates that double capture populates the symmetrical ($n=9, n'=10$) configuration

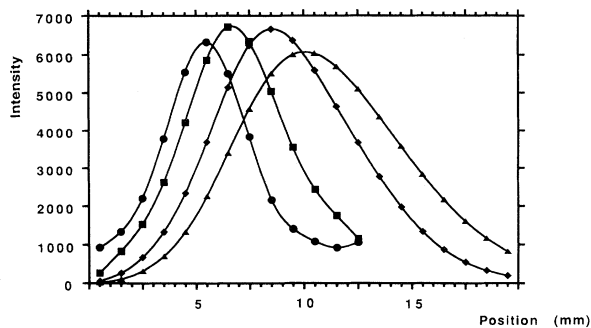


FIG. 5. Simulated growing up and decaying curves of the Kr XVII 13-14 transition convoluted by the gas jet and optical window, assuming a single initial population in quantum number $n = 14$ (●); $n = 16$ (■); $n = 18$ (◆); $n = 19$ (▲).

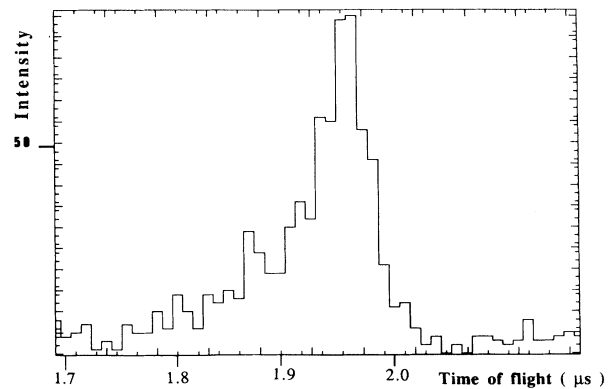


FIG. 6. Experimental decay curve of the Kr VII 7-8 recoil ion transition obtained by coincidence between photons and recoil ions.

of Kr XVII, and a subsequent mixing mechanism between symmetrical and asymmetrical configurations [10] would lead to ($n = 8, n' > 14$) configurations.

From our Ref. 8, Fig. 4, giving the recoil-ion charge distribution in coincidence with Rydberg emission from Kr^{16+} after $\text{Kr}^{18+} + \text{Kr}$ collisions [(double capture):(total capture)=1:5] and our Ref. 6, Fig. 3, giving the value for the total emission cross section for a double charge transfer $\text{Kr}^{18+} + \text{Kr} \rightarrow \text{Kr}^{16+}$ ($\sigma = 2 \times 10^{-16} \text{ cm}^2$), an approximate value of the emission cross section for the Kr XVII 13-14 transition issued from double capture is deduced to be $0.4 \times 10^{-16} \text{ cm}^2$. This value is much lower than the TDC cross section we measured to be $2.7 \times 10^{-16} \text{ cm}^2$ by coincidence between projectiles Kr^{16+} and recoil ions Kr^{2+} after the collision of Kr^{18+} with Kr.

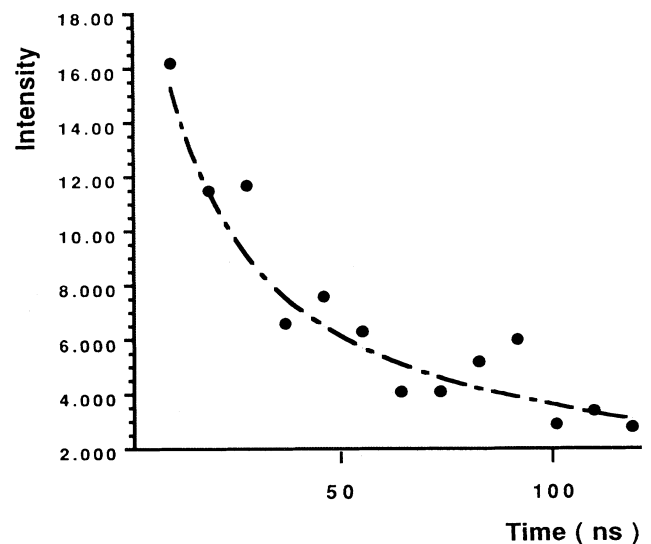


FIG. 7. Decay of the Kr VII 7-8 transition. (●) Experimental decay; (---) simulated decay curve obtained by a Gaussian initial population distribution centered on $n = 20$ with FWHM = 8.

At least two facts contribute to this difference. The emission cross section is less than the excitation cross section and the broadness of the n distribution possibly spreads up to $n > 19$, giving rise to infrared transitions which are outside our spectrometer range. In order to be more complete, larger-range spectroscopy using coincidence techniques would greatly improve the study of double-capture mechanisms.

Figure 6 shows the decay curve of a Kr VII 7-8 recoil-ion transition in a $\text{Kr}^{17+} + \text{Kr}$ collision obtained by coincidence between recoil-ion photons and the recoil-ion charge state using the procedure exposed in the Sec. II. Figure 7 compares a theoretical decay curve simulation and the experimental results. We found that the best fit is obtained for a Gaussian initial population distribution

centered on $n = 20$ with full width at half maximum (FWHM) = 8. This confirms that Rydberg electrons can be recaptured by the target in very high Rydberg levels.

ACKNOWLEDGMENTS

The authors would like to thank T. Lamy, A. Brenac, and G. Lamboley for their assistance in running the ECR ion source of LAGRIPPA, joint laboratory of the CEA and the CNRS (Grenoble, France). The Laboratoire de Spectrometrie Ionique et Moleculaire is "Unité Recherche Associée au CNRS no. 171." The Laboratoire de Traitement du Signal et Instrumentation is "Unité Recherche Associée au CNRS no. 842."

-
- [1] R. K. Janev and H. Winter, *Phys. Rep.* **117**, 265 (1985).
 - [2] C. Harel and H. Jouin, *Europhys. Lett.* **11**, 121 (1990).
 - [3] H. Cederquist *et al.*, *Phys. Rev. A* **46**, 2592 (1992).
 - [4] A. Niehaus, *J. Phys. B* **19**, 2925 (1986).
 - [5] A. Delon, S. Martin, A. Denis, Y. Ouerdane, M. Carré, J. Désesquelles, and M. C. Buchet-Poulizac, *Radiat. Eff. Defects Solids* **126**, 337 (1993).
 - [6] S. Martin, A. Denis, Y. Ouerdane, A. Salmoun, A. El. Motassadeq, J. Désesquelles, M. Druetta, D. Church, and T. Lamy, *Phys. Rev. Lett.* **64**, 2633 (1990).
 - [7] S. Martin, A. Denis, J. Désesquelles, and Y. Ouerdane, *Phys. Rev. A* **42**, 6564 (1990).
 - [8] S. Martin, A. Denis, Y. Ouerdane, and M. Carré, *Phys. Lett. A* **165**, 441 (1992).
 - [9] P. Roncin, H. Laurent, L. Guillemot, M. N. Gaboriaud, and M. Barat, *Z. Phys. D* **21**, S93 (1991).
 - [10] H. Bachau, P. Roncin, and C. Harel, *J. Phys. B* **25**, L109 (1992).
 - [11] S. M. Younger and W. L. Wiese, *Phys. Rev. A* **17**, 1944 (1978).
 - [12] D. Dijkkamp *et al.*, *J. Phys. B* **18**, 4763 (1985).